Characteristic findings in images of extra-pancreatic lesions associated with autoimmune pancreatitis

Short title: Diagnostic imaging characteristics of AIP

Yasunari Fujinaga[a], Masumi Kadoya[a], Shigeyuki Kawa[b], Hideaki Hamano[c], Kazuhiko Ueda[a], Mitsuhiro Momose[a], Satoshi Kawakami[a], Sachie Yamazaki[a], Tomoko Hatta[a], Yukiko Sugiyama[a]

[a] **Department of Radiology, Shinshu University School of Medicine**

[b] **Center of Health, Safety and Environmental Management, Shinshu University**

[c] **Department of Medicine, Gastroenterology, Shinshu University School of Medicine, 3-1-1 Asahi, Matsumoto, 390-8621, Japan**

Abbreviations: AIP; autoimmune pancreatitis, CT; computer-assisted tomography, Ga-67; gallium-67, LIP; lymphocytic interstitial pneumonia, MRI; magnetic resonance imaging, MRCP;magnetic resonance cholangiopancreatography, NSIP; nonspecific interstitial pneumonia, PSC; primary sclerosing cholangitis.

Correspondence: Yasunari Fujinaga,

Department Radiology, Shinshu University School of Medicine, 3-1-1 Asahi,

Matsumoto 390-8621, Japan. (e-mail: fujinaga@shinshu-u.ac.jp). Telephone number:

+81-263-37-2650. Fax number: +81-263-37-3087

Abstract

Purpose: Autoimmune pancreatitis is a unique form of chronic pancreatitis characterized by a variety of extra-pancreatic involvements which are frequently misdiagnosed as lesions of corresponding organs. The purpose of this study was to clarify the diagnostic imaging features of extra-pancreatic lesions associated with autoimmune pancreatitis. **Materials and methods:** We retrospectively analyzed diagnostic images of 90 patients with autoimmune pancreatitis who underwent computer-assisted tomography, magnetic resonance imaging, and/or gallium-67 scintigraphy before steroid therapy was initiated. **Results:** AIP was frequently (92.2%) accompanied by a variety of extra-pancreatic lesions, including swelling of lachrymal and salivary gland lesions (47.5%), lung hilar lymphadenopathy (78.3%), a variety of lung lesions (51.2%), wall thickening of bile ducts (77.8%), peri-pancreatic or para-aortic lymphadenopathy (56.0%), retroperitoneal fibrosis (19.8%), a variety of renal lesions (14.4%), and mass lesions of the *ligamentum teres* (2.2%). Characteristic findings in CT and MRI included lymphadenopathies of the hilar, peri-pancreatic, and para-aortic regions; wall thickening of the bile duct; and soft tissue masses in the kidney, ureters, aorta, paravertebral region, *ligamentum teres*, and orbit. **Conclusions:** Recognition of the diagnostic features in the images of various involved organs will assist in the diagnosis of autoimmune pancreatitis and in differential diagnoses between autoimmune pancreatitis-associated extra-pancreatic lesions and lesions due to other pathologies.

1. Introduction

Autoimmune pancreatitis (AIP) is a unique form of chronic pancreatitis characterized by a preponderance of elderly male sufferers, minimal abdominal pain, irregular narrowing of the main pancreatic duct, and swelling of the pancreatic parenchyma [1-12]. The pathogenesis is thought to involve an autoimmune mechanism based on the presence of various serum autoantibodies, hypergammaglobulinemia, histological evidence of lymphoplasmacytic inflammation and fibrosis, and a favorable response to glucocorticoid treatment [13-21]. This disease has been occasionally misdiagnosed as pancreatic cancer, leading to unnecessary surgery [22, 23]. It is therefore imperative to improve the diagnostic accuracy for AIP.

The characteristic features of AIP include a high serum IgG4 concentration and complications involving various extra-pancreatic lesions. Over 90% of patients exhibit high serum IgG4 concentrations, reflecting infiltration of abundant IgG4-bearing plasma cells and disease activity [11] in the pancreatic lesion [12, 18]. Thus, a serum assay for IgG4 provides a useful tool for the diagnosis and monitoring of this disease. In addition, abundant IgG4-bearing plasma cells are a histological hallmark that can be used in differentiating between AIP and malignant conditions.

Other prominent features of AIP involve a variety of extra-pancreatic complications, including sclerosing cholangitis [2, 7, 17, 19, 20], lachrymal and salivary gland abnormalities [18, 24], hypothyroidism [25], hilar lymphadenopathy [26], retroperitoneal fibrosis [12, 17, 27-29], interstitial pneumonia [30, 31], and tubulointerstitial nephritis [32, 33]. Some of these extra-pancreatic lesions exhibit

4

pathologies similar to those found in pancreatic lesions, including infiltration of abundant IgG4-bearing plasma cells [12, 18, 26, 29]. In addition, the presence of multiple extra-pancreatic lesions suggests a systemic disease associated with IgG4 [12]. Most reports regarding AIP-associated extra-pancreatic lesions have been published as single cases, small series of cases, or cases restricted to specific lesions. There have been only a few detailed reports addressing the broad spectrum of manifestations [34, 35, 36], particularly with regard to imaging that might be useful in the diagnosis of extra-pancreatic lesions associated with AIP.

It is uncertain whether there are imaging characteristics that might be useful for differentiation between IgG4-related extra-pancreatic lesions and other diseases affecting the same organs. In this study, we aimed to characterize and identify useful imaging features of a large cohort in the diagnosis of extra-pancreatic manifestations of AIP to differentiate them from other diseases affecting the same organs.

2. Materials and methods

We systematically reviewed diagnostic images for 90 patients with AIP, 75 men and 15 women aged 38-79 (median age, 63.1 years old), treated in our hospital and affiliated hospitals between September, 1994 and March, 2008. Diagnosis of AIP was based on the criteria proposed by the Japanese Pancreatic Society in 2002 [37] and the revised version in 2006 [38].

We analyzed images from computer-assisted tomography (CT), magnetic resonance imaging (MRI), and/or gallium-67 (Ga-67) scintigraphy that were taken at admission or

during an active stage of the disease before the initiation of steroid therapy. CT

examination was performed with single-detector row helical CT (HiSpeed Advantage;

GE Medical Systems, Milwaukee, WI, USA) from 1994 to 2003 and with multi-

detector row helical CT from 2003 to 2008 (LightSpeed Ultra or LightSpeed VCT; GE

Medical Systems, Milwaukee, WI, USA). Because of the length of the period under

review, the model of the CT scanner, slice thickness (1.25 – 10 mm) and the protocol of

the contrast-enhanced CT varied. MRI was performed with a 1.5-T superconductor unit

(Magnetom Symphony, Siemens Medical Solution, Erlangen, Germany) from 1994 to

2006 and with a 3-T superconductor unit (Magnetom Trio, Siemens Medical Solution,

Erlangen, Germany) from 2007 to 2008. The slice thickness (2 – 10 mm), image

sequence and the protocol of the contrast-enhanced MRI varied for the same reason.

Ga-67 scintigraphy was performed with a single-head rectangular gamma camera

(SNC-510R; Shimazu, Japan) from 1994 to 2002 and a triple-head rotating gamma

camera (PRISM IRIX; Philips Medical Systems, Best, The Netherlands) or a large field-

of-view dual-detector gamma camera with a mounted CT scanner (Millennium VG, GE

Medical Systems, Milwaukee, WI, USA) from 2003 to 2008.

Abdominal and thoracic CT images were available in all 90 and 69 patients,

respectively. Abdominal MRI and neck MRI were available in 78 and 40 patients,

respectively. Ga-67 scintigram was available in 80 patients. Systemic image analysis

using CT, MRI and Ga-67 was performed, even if they showed no specific symptoms of

the extra-pancreatic organs, because lesions in extra-pancreatic organs found on images

were not always associated with symptoms. Image findings were reviewed by two

radiologists (Y.F. and M.K.) in consensus.

3. Results

Among 90 patients, 83 (92.2 %) had various extra-pancreatic lesions associated with

AIP. We summarize the distribution and frequency of the extra-pancreatic lesions in

Table 1, and describe the details of each type of lesion in the following sections.

3.1. Lachrymal and salivary gland lesions

Among 80 patients that underwent Ga-67 scintigraphy, 38 (47.5%) had lachrymal or

salivary gland lesions (Table 1). Two submandibular lesions and two lachrymal lesions

were histopathologically proven by biopsy, and other lesions were clinically diagnosed.

Ga-67 scintigraphy showed increased uptake in either the lachrymal or salivary gland in

36 of these 38 patients (95%) (Fig. 1a). The submandibular gland was involved in 29

patients (76%), the lachrymal gland in 27 (75%), the parotid gland in 5 (13%), and the

sublingual gland in 2 (5%). Increased uptakes were symmetrical in all except three of

the patients; one showed right-side-dominant uptake at the lachrymal gland, one showed

left-side-dominant uptake at the lachrymal gland, and one showed right-side-dominant

uptake at the submandibular gland. After corticosteroid therapy, increased uptake of all

lesions was disappeared.

Neck MRI was performed in 40 patients in whom increased uptake was seen on

Ga-67 scintigraphy or clinical symptoms were described. The MRIs showed a bilateral

7

homogeneous swelling of the glands without a discernable mass (Fig. 1b) in 14 patients,

unilateral swelling in two patients and normal findings in 24 patients. Biopsies

performed in 2 patients showed that the swelling submandibular glands contained

abundant IgG4-bearing plasma cells. No lesions showed the salt-and-pepper appearance

characteristic of Sjoegren's syndrome [39].

3.2. Hilar lymphadenopathy

Hilar lymphadenopathy was revealed in 54 of 69 patients (78%) undergoing

thoracic CT (Table 1), and contrast-enhanced CT was used to improve the visualization

of bilateral hilar lymphadenopathy (Fig. 2a). Ga-67 scintigraphy also showed marked

bilateral hilar uptake in 60 of 80 cases (75%) (Fig. 2b) (Table 1). After corticosteroid

therapy, bilateral hilar lymphadenopathy disappeared in all cases. No biopsies were

taken. There was no unilateral lymphadenopathy found by CT or Ga-67 scintigraphy.

3.3 Pulmonary abnormalities

Lung lesions were revealed in 25 of 46 patients (54%) undergoing thin-slice CT

(Table 1). Five patients were histopathologically proven by biopsy and 20 were

clinically diagnosed. There were four types of CT findings, including nodular lesions,

bronchial thickening, interlobular thickening, and consolidation. Nodular lesions (3 to

26 millimeters in diameter) were found in 18 (39%) (Fig. 3a), bronchial thickening in

14 (30%) (Fig. 3b), interlobular thickening in 7 (15%) (Fig. 3c), and consolidations in 2

(4%) (Fig. 3d). Almost all the nodular lesions were located adjacent to the pleura. Two

or more types of lesions coexisted in 14 cases (Fig. 3e). All lesions diminished or disappeared after corticosteroid therapy.

3.4. Bile duct abnormalities

CT or MRI showed extra-pancreatic bile duct lesions in 63 of 81 patients (78%) (Table 1); nine patients were excluded due to unavailable CT or MR images, or if the detailed analysis of bile ducts was difficult due to occlusion by drainage tubes. Biopsies were performed in 19 cases, and abundant IgG4-bearing plasma cell infiltration was evident. Other 44 cases were clinically diagnosed. Almost all bile duct abnormalities in these 63 patients included extensive wall thickening, with occlusion of the intrahepatic bile duct in 23 (28%) and of the common hepatic or intra-pancreatic common bile duct in 37 (46%) (Fig. 4). MRI clearly demonstrated these lesions (Fig. 5), and showed prominent wall thickening with a laminar structure (Fig. 6) in some cases and focal wall thickening of the common bile duct in 5 (6%). Magnetic resonance cholangiopancreatography (MRCP) was performed in 66 patients and showed intrahepatic bile duct stenosis, which mimicked primary sclerosing cholangitis (PSC) in 6 (9%). Severe bile duct dilatation was observed when the pancreas head was swollen.

3.5 Peri-pancreatic and para-aortic lymphadenopathy

CT or MRI showed peri-pancreatic or para-aortic lymphadenopathy in 51 of 90 cases (57%) (Table 1). All lesions were clinically diagnosed. CT clearly demonstrated lymph

node swelling that produced high signal intensities on diffusion-weighted MRI (Fig 7a, b). No biopsies were taken, but corticosteroid therapy was effective for all lesions.

3.6. Renal lesions

CT or MRI showed renal lesions in 13 of 90 cases (14%), including parenchymal lesions in 10 and hilar lesions in 3 (Fig. 2c) (Table 1). Four renal parenchymal lesions and 1 hilar lesion were diagnosed by biopsies and other 12 cases were clinically diagnosed. All 10 parenchymal lesion cases had multiple bilateral lesions, and 2 had unilateral renal atrophy. Contrast-enhanced CT showed renal parenchymal lesions as slightly enhanced wedge- or node-shaped lesions. Multiphase dynamic contrast-enhanced CT were performed in 5 of 10 patients and revealed that the shapes changed over time and were ill-defined in the delayed phase (Fig. 8) in all cases. Renal lesions were unclear on T1-weighted MR images, but had slightly high intensity on T2-weighted MR images, and high intensity on diffusion-weighted images. These lesions were wedge- or node-shaped on dynamic multiphase T1-weighted images. CT and MRI showed prominent and diffuse renal pelvic wall thickening in renal hilus lesions. Ga-67 scintigraphy showed inincrease uptake in all renal lesions.

3.7. Retroperitoneal lesions

CT showed retroperitoneal fibrosis in 17 of the 86 cases for which findings were available (20%) (Table1), including a soft tissue density around the aorta in 11 (Fig. 9a), soft tissue masses around both ureters in 3 (Fig. 9b), paravertebral masses in 2, a pelvic

10

retroperitoneal mass in 1, and increased fat density around the superior mesenteric

artery in 1 (Fig. 9c). The biopsy specimens from 3 para-aortic lesion cases and 2 peri-

ureteral lesion cases showed abundant IgG4 plasma cell infiltration. A paravertebral

mass and pelvic retroperitoneal mass were observed together in the same patient (Fig.

2d, e). Three of 11 cases with para-aortic lesions had aortic aneurysms. One of 3 cases

with peri-ureteral lesions had hydronephrosis.

3.8. Other lesions

CT or MRI showed *ligamentum teres* lesions in 2 of the 90 cases (2%) (Table 1).

Both lesions were clinically diagnosed and no biopsy was taken. These lesions showed

a spindle-shaped soft tissue mass on CT, hypointense mass on T1-weighted image, and

hyperintense mass on T2-weighted images (Fig. 10).

Ga-67 scintigraphy exhibited Ga-67 accumulation in the prostate in 8 of 80 cases

(10%) (Table 1). Biopsy specimens from two patients showed abundant IgG4-positive

plasma cells and lymphocyte infiltration. Other six patients were clinically diagnosed.

Diffusion-weighted MRI showed prostatic swelling with high intensity signals (Fig. 11),

which mimicked prostate cancer or prostatitis.

4. Discussion

The present study demonstrated some characteristics found in images of various

extra-pancreatic lesions associated with AIP. Because they favorably respond to

corticosteroid therapy, it is important to differentiate these IgG4-related extra-pancreatic

lesions from other diseases that might affect the same organs, including Sjögren's

syndrome, sarcoidosis, and primary sclerosing cholangitis. In general, differentiation has previously been based on histological findings and the response to corticosteroid therapy. In this study, we aimed to identify characteristics in images that would be useful for the diagnosis and differentiation of AIP-related lesions with noninvasive imaging.

The major causes of lachrymal and salivary gland swelling include Sjögren's syndrome, Mikulicz disease, or Küttner tumors. Recent reports have shown that high serum IgG4 concentrations and abundant IgG4-bearing plasma cell infiltration were associated with Mikulicz disease and Küttner tumors, but not Sjögren's syndrome [40-42]. In our series, lachrymal and salivary gland lesions responded well to corticosteroid therapy, and thus were similar to those described in Mikulicz disease and Küttner tumors. For this reason, we speculate that the lachrymal and salivary gland lesions associated with AIP may arise from the same or similar systemic conditions as those associated with Mikulicz disease and Küttner tumors.

In our series, 95 % of the patients presented with lachrymal or submandibular gland enlargement and only five patients (12.5%) presented with parotid gland enlargement. By contrast, patients with Sjögren's syndrome frequently present with parotid gland enlargement. This difference in the distribution of lesions might be important for the differentiation of AIP-associated lesions and Sjögren's syndrome lesions. In addition, a salt-and-pepper appearance is typically found on the MRIs in Sjögren's syndrome [38]. By contrast, the salivary gland lesions in our series always exhibited homogeneous swelling. This difference in imaging characteristics should be helpful for the

differentiation between the two diagnoses. Furthermore, we found that increased Ga-67 uptake by the pancreas and the presence of other extra-pancreatic lesions are indicative of an AIP diagnosis.

Hilar Ga-67 accumulation has been reported in other diseases, including sarcoidosis or primary biliary cirrhosis. Thus, it is necessary to differentiate between these diseases and AIP. Saegusa et al. reported that hilar and pancreatic Ga-67 accumulations are characteristic features of AIP during the active stage of the disease [26]. In our series, almost all patients had Ga-67 accumulation in the pancreas and, concomitantly, in extra-pancreatic lesions, including the lachrymal gland, salivary gland, lung, retroperitoneum and/or prostate. Systemic Ga-67 accumulation was helpful for diagnosing AIP-associated hilar lymphadenopathy. In addition, a normal serum ACE value might be helpful for the exclusion of sarcoidosis.

Radiologically, lung lesions associated with AIP were similar to those indicative of nonspecific inflammatory nodules, chronic bronchitis, chronic bronchiolitis, nonspecific interstitial pneumonia (NSIP), and lymphocytic interstitial pneumonia (LIP). All these lesions had a tendency to spread in the interstitial space of the lung, including the lymphoid channel. At present, we have no clear understanding of the relationship between AIP-related lung lesions and other lung lesions; this remains an issue for future study.

Bile duct abnormality was the most common abdominal finding associated with AIP in the present study, though Shoe et al. reported that retroperitoneal fibrosis was most frequently seen among abdominal lesions in AIP patients [36]. We suspect that

differences in the case numbers and study methods were the cause of this disparity. The bile duct wall thickening found in AIP-associated lesions has not been reported in primary sclerosing cholangitis or bile duct carcinoma. In the absence of swelling of the pancreas head, intrahepatic bile duct dilatation was mild, regardless of the bile duct wall thickness. These findings were helpful in differentiating between AIP-associated lesions and those associated with PSC or bile duct carcinoma. In addition, a favorable response to corticosteroid therapy was a distinguishing factor between AIP- and PSC-related lesions, although some sclerosing cholangitis can be cured by steroid therapy [7,17,20,43,44]. However, pancreatic and bile duct lesions had similar pathologies [27, 45- 47]; thus, when diagnosis with imaging is difficult, a biopsy should be performed. Endoscopic retrograde cholangiopancreatography (ERCP) has also been reported to be useful for differentiating between AIP- and PSC-associated lesions [48].

AIP-associated peri-pancreatic or para-aortic lymphadenopathy is not easily distinguished from inflammatory lymph node swelling and malignant lymphomas. We found that the coexistence of lymphadenopathies and pancreatic lesions is the only distinguishing feature of AIP.

Poorly enhanced multiple wedge-shaped or round lesions associated with AIP are not easily differentiated from those associated with pyelonephritis or infarctions [49, 50]. We found graduated enhancement on dynamic contrast-enhanced CTs or MRIs and increased Ga-67 uptake; these characteristics might be specific for AIP-associated renal lesions. Renal hilus lesions are often difficult to differentiate from urothelial tumors,

retroperitoneal fibrosis, and lymphomas. Our results suggested that the observation of a combination of pancreatic and extra-pancreatic lesions would be indicative of AIP.

There are only a few reports that describe para-aortic soft tissue masses associated with AIP [12, 36, 51, 52]. Results from those studies were consistent with our findings of a broad homogeneous soft tissue mass along the aorta. This finding should be useful for differentiating AIP from other inflammatory conditions and retroperitoneal tumors. However, the diagnosis is often difficult when a slightly increased density of fat is observed. Kasashima et al. reported that one type of inflammatory abdominal aortic aneurysm was IgG4-related and may be the result of IgG4-related peri-aortitis or retroperitoneal fibrosis [53]. In our series, 3 of 11 patients with para-aortic soft tissue thickening were diagnosed with aortic aneurysms. Hence, IgG4-related para-aortic soft tissue thickening might increase the risk of developing an aortic aneurysm.

This was the first report of AIP-associated *ligamentum teres* lesions. They were a rare (2%) but characteristic finding, and both lesions disappeared after corticosteroid therapy. If the Ga-67 scintigraphy shows increased uptake in these lesions, extra-pancreatic lesions associated with AIP can be easily differentiated from other tumors or tumor-like lesions, such as metastatic tumors, leiomyoma, leiomyosarcoma, and extramedullary hematopoiesis because Ga-67 accumulation is very rare in these tumors.

We found prostatic lesions by Ga-67 scintigraphy and diffusion-weighted MRIs. These were often difficult to differentiate from prostate cancer and prostatitis. We found that biopsy was mandatory for confirming abundant IgG4-positive plasma cells and lymphocyte infiltration; in addition, a favorable response to corticosteroid therapy was

helpful in identifying AIP. To date, a few AIP-associated prostate lesions have been reported, but detailed image findings have not been previously described [54, 55].

In this study, we described variable findings of multiple AIP-associated soft tissue masses in the kidney, around the ureter, aorta, paravertebral region, *ligamentum teres*, and orbit. These lesions resembled inflammatory pseudotumors because they frequently contained abundant plasma cell infiltration. Diagnostic imaging played an important role in detecting these lesions, and the characteristic finding of multiple lesions may provide a useful tool for the correct diagnosis of AIP-associated lesions.

AIP and AIP-associated extra-pancreatic lesions are frequently found simultaneously; thus, it is important to examine all other organs when a pancreatic lesion is found. However, these lesions are not always synchronous; thus, successive diagnostic imaging should be mandatory for the detection of newly occurring AIP-associated lesions.

Our study had some limitations, mainly due to using variable models as well as variable scan protocols of CT, MRI and gamma camera because of the length of period reviewed in our retrospective study. Furthermore, all patients were not checked by every image test. Another limitation was that many extra-pancreatic lesions were not histopathologically proven. Therefore, there is a problem that some the lesions improved by corticosteroid therapy might not be always AIP related extra-pancreatic lesions. Conversely, some of the lesions that were not improved by corticosteroid therapy might include AIP related extra-pancreatic lesions. This problem was not analyzed in this study.

5. Conclusion

AIP is accompanied by various extra-pancreatic lesions and characterized by a variety of image findings. Diagnostic imaging plays an important role in the comprehensive evaluation of these lesions. Radiologists and physicians should keep in mind that multiple lesions may or may not be synchronous under different conditions.

References

[1]. Sarles H, Sarles JC, Muratore R, Guien C. Chronic inflammatory sclerosis of the pancreas—an autonomous pancreatic disease? Am J Dig Dis 1961; 6: 688-98.

[2]. Kawaguchi K, Koike M, Tsuruta K, Okamoto A, Tabata I, Fujita N. Lymphoplasmacytic sclerosing pancreatitis with cholangitis: a variant of primary sclerosing cholangitis extensively involving pancreas. Hum Pathol 1991; 22: 387-95.

[3]. Toki F, Kozu T, Oi I, Nakasato T, Suzuki M, Hanyu F. An unusual type of chronic pancreatitis showing diffuse irregular narrowing of the entire main pancreatic duct on ERCP—a report of four cases. Endoscopy 1992; 24: 640. [abstract]

[4]. Wakabayashi T, Motoo Y, Kojima Y, Makino H, Sawabu N. Chronic pancreatitis with diffuse irregular narrowing of the main pancreatic duct. Dig Dis Sci 1998; 43: 2415-25.

[5]. Horiuchi A, Kaneko T, Yamamura N, et al. Autoimmune chronic pancreatitis simulating pancreatic lymphoma. Am J Gastroenterol 1996; 91: 2607-9.

[6]. Horiuchi A, Kawa S, Akamatsu T, et al. Characteristic pancreatic duct appearance in autoimmune chronic pancreatitis: a case report and review of the Japanese literature. Am J Gastroenterol 1998; 93: 260-3.

[7]. Erkelens GW, Vleggaar FP, Lesterhuis W, van Buuren HR, van der Werf SD. Sclerosing pancreato-cholangitis responsive to steroid therapy. Lancet 1999; 354: 43-4.

[8]. Okazaki K, Uchida K, Ohana M, et al. Autoimmune-related pancreatitis is associated with autoantibodies and a Th1/Th2-type cellular immune response. Gastroenterology 2000; 118: 573-81.

[9]. Okazaki K, Chiba T. Autoimmune related pancreatitis. Gut 2002; 51: 1-4

[10]. Uchida K, Okazaki K, Konishi Y, et al. Clinical analysis of autoimmune-related pancreatitis. Am J Gastroenterol 2000; 95: 2788-94.

[11]. Hamano H, Kawa S, Horiuchi A, et al. High serum IgG4 concentrations in patients with sclerosing pancreatitis. N Engl J Med 2001; 344: 732-8.

[12]. Hamano H, Kawa S, Ochi Y, et al. Hydronephrosis associated with retroperitoneal fibrosis and sclerosing pancreatitis. Lancet 2002, 359: 1403-4.

[13]. Yoshida K, Toki F, Takeuchi T, Watanabe S, Shiratori K, Hayashi N. Chronic pancreatitis caused by an autoimmune abnormality. Proposal of the concept of autoimmune pancreatitis. Dig Dis Sci 1995; 40: 1561-8.

[14]. Ito T, Nakano I, Koyanagi S, et al. Autoimmune pancreatitis as a new clinical entity. Three cases of autoimmune pancreatitis with effective steroid therapy. Dig Dis Sci 1997; 42: 1458-68

[15]. Kawa S, Ota M, Yoshizawa K, et al. HLA DRB10405-DQB10401 haplotype is associated with autoimmune pancreatitis in the Japanese population. Gastroenterology 2002; 122: 1264-9.

[16]. Horiuchi A, Kawa S, Hamano H, Hayama M, Ota H, Kiyosawa K. ERCP features in 27 patients with autoimmune pancreatitis. Gastrointest Endosc 2002; 55: 494-499

[17]. Hirano K, Shiratori Y, Komatsu Y, et al. Involvement of the biliary system in autoimmune pancreatitis: a follow-up study. Clin Gastroenterol Hepatol 2003; 1: 453-564

[18]. Kamisawa T, Funata N, Hayashi Y, et al. Close relationship between autoimmune pancreatitis and multifocal fibrosclerosis. Gut 2003; 52: 683-7.

[19]. Nakazawa T, Ohara H, Yamada T, et al. Atypical primary sclerosing cholangitis cases associated with unusual pancreatitis. Hepatogastroenterology 2001; 48: 625-30.

[20]. Horiuchi A, Kawa S, Hamano H, Ochi Y, Kiyosawa K. Sclerosing pancreato-cholangitis responsive to corticosteroid therapy: report of 2 case reports and review. Gastrointest Endosc 2001; 53: 518-22.

[21]. Notohara K, Burgart LJ, Yadav D, Chari S, Smyrk TC. Idiopathic chronic pancreatitis with periductal lymphoplasmacytic infiltration: clinicopathologic features of 35 cases. Am J Surg Pathol 2003; 27: 1119-27.

[22]. Hardacre JM, Iacobuzio-Donahue CA, et al. Results of pancreaticoduodenectomy for lymphoplasmacytic sclerosing pancreatitis. Ann Surg 2003; 237: 853-9.

[23]. Kamisawa T, Egawa N, Nakajima H, Tsuruta K, Okamoto A, Kamata N. Clinical difficulties in the differentiation of autoimmune pancreatitis and pancreatic carcinoma. Am J Gastroenterol 2003; 98: 2694-9.

[24]. Nakano S, Takeda I, Kitamura K, Watahiki H, Iinuma Y, Takenaka M. Vanishing tumor of the abdomen in patient with Sjögren's syndrome. Am J Dig Dis 1978; 23 (Suppl): 75S-79S.

[25]. Komatsu K, Hamano H, Ochi Y, et al. High prevalence of hypothyroidism in patients with autoimmune pancreatitis. Dig Dis Sci 2005; 50: 1052-7.

[26]. Saegusa H, Momose M, Kawa S, et al. Hilar and pancreatic gallium-67 accumulation is characteristic feature of autoimmune pancreatitis. Pancreas 2003; 27:20-5.

[27]. Uchida K, Okazaki K, Asada M, et al. Case of chronic pancreatitis involving an autoimmune mechanism that extended to retroperitoneal fibrosis. Pancreas 2003; 26: 92-4.

[28]. Fukukura Y, Fujiyoshi F, Nakamura F, Hamada H, Nakajo M. Autoimmune pancreatitis associated with idiopathic retroperitoneal fibrosis. AJR Am J Roentgenol 2003; 181: 993-5.

[29]. Kamisawa T, Nakajima H, Egawa N, Funata N, Tsuruta K, Okamoto A. IgG4-related sclerosing disease incorporating sclerosing pancreatitis, cholangitis, sialadenitis and retroperitoneal fibrosis with lymphadenopathy. Pancreatology 2006; 6: 132-7.

[30]. Taniguchi T, Ko M, Seko S, et al. Interstitial pneumonia associated with autoimmune pancreatitis. Gut 2004; 53: 770.

[31]. Hirano K, Kawabe T, Komatsu Y, et al. High-rate pulmonary involvement in autoimmune pancreatitis. Intern Med J 2006; 36: 58-6.

[32]. Takeda S, Haratake J, Kasai T, Takaeda C, Takazakura E. IgG4-associated idiopathic tubulointerstitial nephritis complicating autoimmune pancreatitis. Nephrol Dial Transplant 2004; 19: 474-6.

[33]. Uchiyama-Tanaka Y, Mori Y, Kimura T, et al. Acute tubulointerstitial nephritis associated with autoimmune-related pancreatitis. Am J Kidney 2004; Dis 43: e18-25.

[34]. Ohara H, Nakazawa T, Sano H, et al. Systemic extrapancreatic lesions associated with autoimmune pancreatitis. Pancreas 2005; 31: 232-7.

[35]. Hamano H, Arakura N, Muraki T, Ozaki Y, Kiyosawa K, Kawa S. Prevalence and distribution of extrapancreatic lesions complicating autoimmune pancreatitis. J Gastroenterol 2006; 41: 1197-205.

[36]. Sohn JH, Byun JH, Yoon SE, et al. Abdominal extrapancreatic lesions associated with autoimmune pancreatitis: radiological findings and changes after therapy. Eur J Radiol. 2008;67:497-507.

[37]. Members of the Criteria Committee for Autoimmune Pancreatitis of the Japan Pancreas Society. Diagnostic criteria for autoimmune pancreatitis by the Japan Pancreas Society (in Japanese with English abstract). Suizo (J Jpn Pancreas Soc) 2002;17:585–7.

[38]. Okazaki K, Kawa S, Kamisawa T, et al. Clinical diagnostic criteria of autoimmune pancreatitis—revised proposal. *J Gastroenterol* 2006; 41: 626-31.

[39]. Takashima S, Takeuchi N, Morimoto S, et al. MR imaging of Sjögren syndrome: correlation with sialography and pathology. J Comput Assist Tomogr 1991; 15:393-400.

[40]. Yamamoto M, Ohara M, Suzuki C, et al. Elevated IgG4 concentrations in serum of patients with Mikulicz's disease. Scand J Rheumatol 2004; 33: 432-3.

[41]. Yamamoto M, Takahashi H, Sugai S, Imai K. Clinical and pathological characteristics of Mikulicz's disease (IgG4-related plasmacytic exocrinopathy). Autoimmun Rev 2006; 4:195-200.

[42]. Kitagawa S, Zen Y, Harada K, et al. Abundant IgG4-positive plasma cell infiltration characterizes chronic sclerosing sialadenitis (Kuttner's tumor). Am J Surg Pathol 2005; 29: 783-91.

[43]. Eerens I, Vanbeckevoort D, Vansteenbergen W, Van Hoe L. Autoimmune pancreatitis associated with primary sclerosing cholangitis: MR imaging findings. Eur Radiol 2001; 11: 1401-4.

[44]. Kuroiwa T, Suda T, Takahashi T, et al. Bile duct involvement in a case of autoimmune pancreatitis successfully treated with an oral steroid. Dig Dis Sci 2002; 47: 1810-6.

[45]. Zen Y, Harada K, Sasaki M, et al. IgG4-related sclerosing cholangitis with and without hepatic inflammatory pseudotumor, and sclerosing pancreatitis-associated sclerosing cholangitis: do they belong to a spectrum of sclerosing pancreatitis? Am J Surg Pathol 2004; 28: 1193-203.

[46]. Uehara T, Hamano H, Kawa S, Sano K, Honda T, Ota H. Distinct clinicopathological entity 'autoimmune pancreatitis-associated sclerosing cholangitis'. Pathol Int 2005; 55:405-11.

[47]. Hamano H, Kawa S, Uehara T, et al. Immunoglobulin G4-related lymphoplasmacytic sclerosing cholangitis that mimics infiltrating hilar

cholangiocarcinoma: part of a spectrum of autoimmune pancreatitis? Gastrointest Endosc 2005; 62: 152-7.

[48]. Nakazawa T, Ohara H, Sano H, et al. Cholangiography can discriminate sclerosing cholangitis with autoimmune pancreatitis from primary sclerosing cholangitis. Gastrointest Endosc 2004; 60:937-44.

[49]. Takahashi N, Kawashima A, Fletcher JG, Chari ST. Renal involvement in patients with autoimmune pancreatitis: CT and MR imaging findings. Radiology 2007; 242: 791-801.

[50]. Saeki T, Nishi S, Ito T, et al. Renal lesions in IgG4-related systemic disease. Intern Med 2007; 46: 1365-71.

[51]. Zen Y, Sawazaki A, Miyayama S, K, Tanaka N, Nakanuma Y. A case of retroperitoneal and mediastinal fibrosis exhibiting elevated levels of IgG4 in the absence of sclerosing pancreatitis (autoimmune pancreatitis). Hum Pathol 2006; 37: 239-43.

[52]. Kamisawa T, Chen PY, Tu Y, Nakajima H, Egawa N. Autoimmune pancreatitis metachronously associated with retroperitoneal fibrosis with IgG4-positive plasma cell infiltration. World J Gastroenterol 2006; 12: 2955-7.

[53]. Kasashima S, Zen Y, Kawashima A, et al. Inflammatory abdominal aortic aneurysm: Close relationship to IgG4-related periaortitis. Am J Surg Pathol 2008; 32:197-204.

[54]. Yoshimura Y, Takeda S, Ieki Y, Takazakura E, Koizumi H, Takagawa K. IgG4-

associated prostatitis complicating autoimmune pancreatitis. Intern Med 2006; 45:

897-901.

[55]. Hamed G, Tsushima K, Yasuo M, et al. Inflammatory lesions of the lung,

submandibular gland, bile duct and prostate in a patient with IgG4-associated

multifocal systemic fibrosclerosis. Respirology 2007; 12: 455-7.

Table1. Summary of the prevalence and distribution of extra-pancreatic lesions

Organ	No. of cases	Percentage
Total extra-pancreatic lesions	83/90	92.2%
Lachrymal or salivary grand	38/80	47.5%
Hilar lymph node (CT)	54/69	78.3%
Hilar lymph node (Ga-67 scintigraphy)	60/80	75%
Lung	25/46	54.3%
Bile duct	63/81	77.8%
Peri-pancreatic or para-aortic lymph node	51/90	57%
Kidneys	13/90	14.4%
Retroperitoneum	17/86	19.8%
Ligamentum teres	2/90	2.2%
Prostate	8/80	10.0%

The total number of examined cases in each row is different among respective lesions because CT, MRI or Ga-67 scintigraphy was not performed in all the organs, and some images were not available.

Figure Legends

(a)   (b)
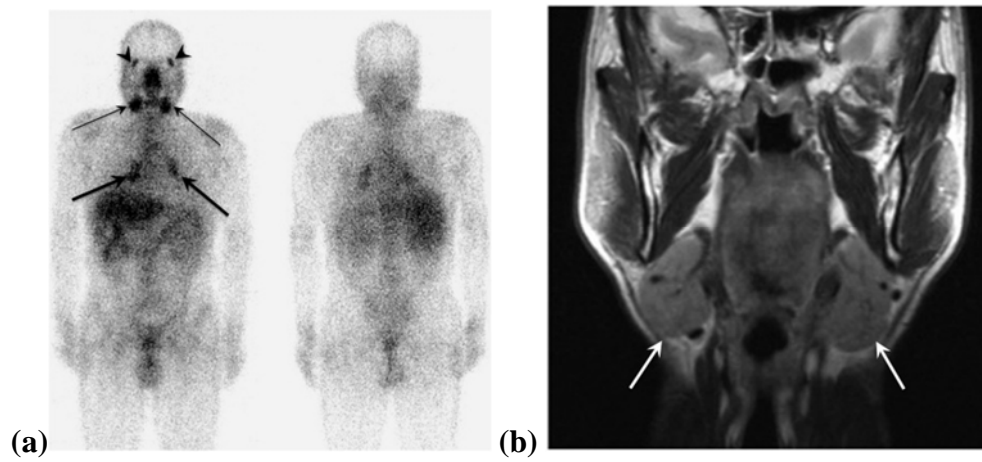
Fig. 1. Lachrymal and salivary lesions in a 67-year-old man visualized with Ga-67

scintigraphy and MRI. **(a)** Ga-67 scintigraphy shows increased uptake in the hilar

(arrows), submandibular (thin arrows), and lachrymal glands (arrow heads). **(b)**

Coronal T2-weighted images show bilateral submandibular gland swellings that

are homogeneous without dilatation of the ducts (white arrows).
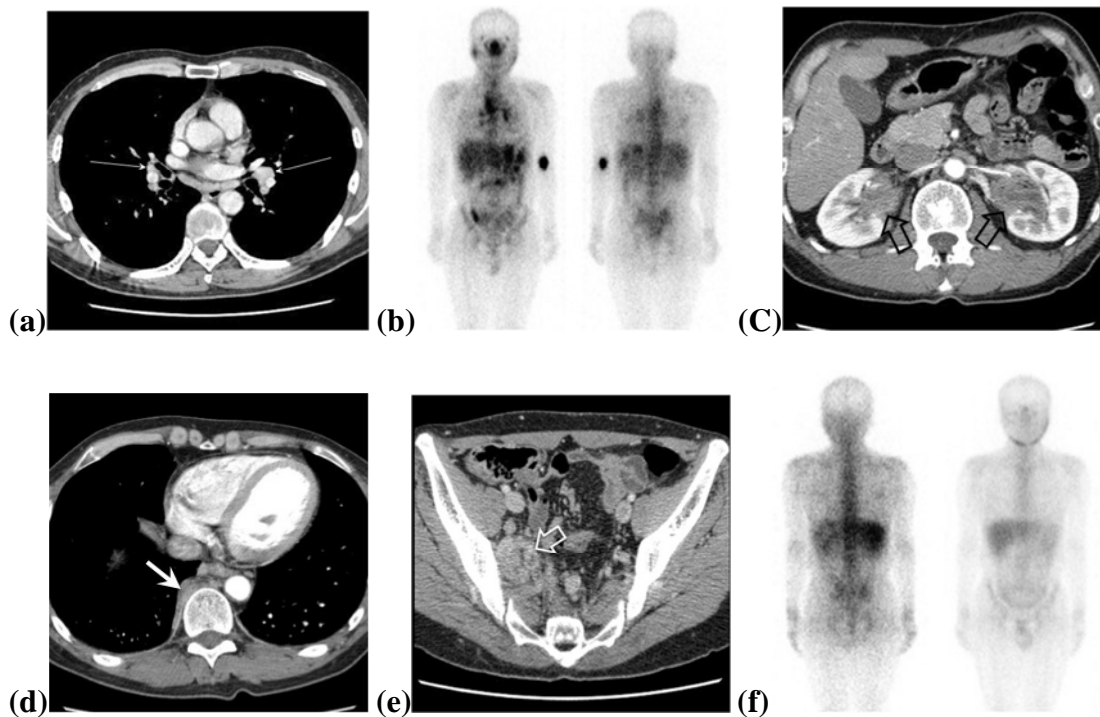
Fig. 2. Hillar lymphadenopathy in a 50-year-old man. (a) Dynamic contrast-enhanced

CT shows hilar lymphadenopathy (long arrows). (b) Ga-67 scintigraphy

demonstrates an increased uptake in right parotid gland and right retroperitoneum,

as well as hilum. (c-e) Another slice of the dynamic contrast-enhanced CT

identifies bilateral renal lesions (open arrows in c), paravertebral mass (white

arrow in d) and retroperitoneal fibrosis (white open arrow in e) (to be describe).

(f) After corticosteroid therapy, the accumulation of Ga-67 disappeared in each

lesion.
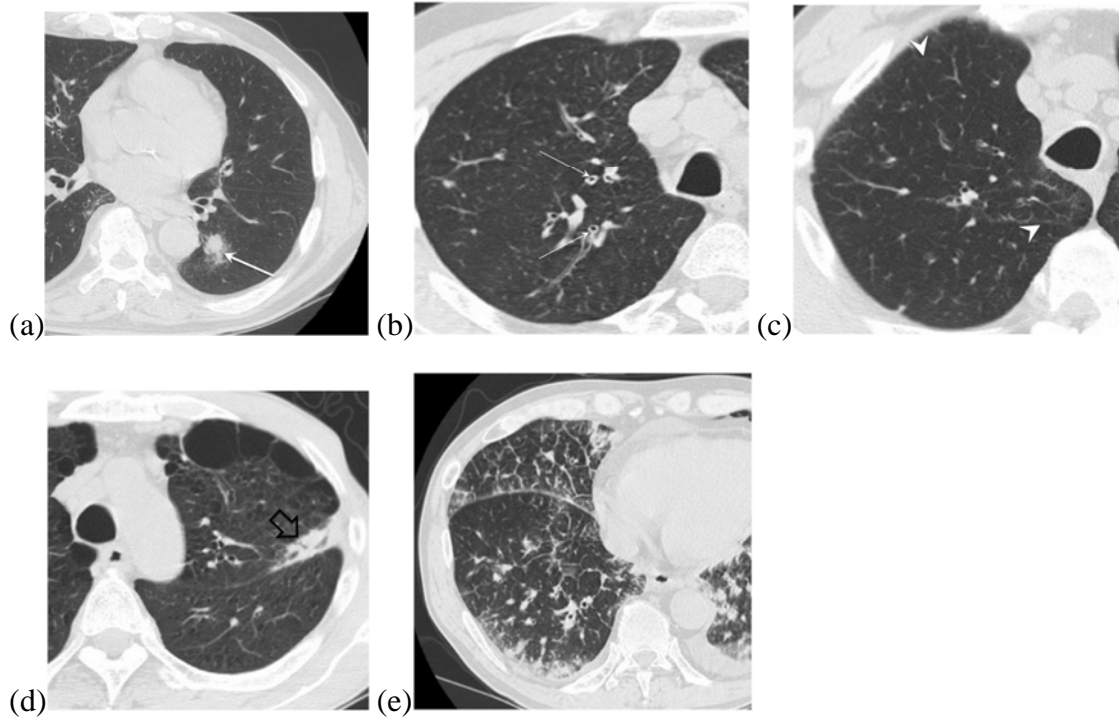
Fig. 3 Lung lesions. (a – d) Thin-sliced CT before corticosteroid therapy shows an

irregular nodular lesion in the left lower lobe (white arrow in a), bronchial

thickening in the right upper lobe (thin white arrows in b), diffuse interlobular

thickening in the right upper lobe (arrow heads in c), and subpleural consolidation

in the left lower lobe (open arrow in d). (e) In another case, a coarse reticulation

consistent with thickening of interlobular septa is mixed with multiple subpleural

consolidations in the right lower lobe.
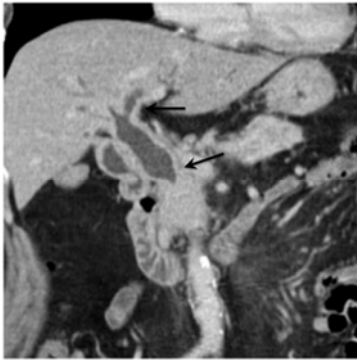
Fig. 4 Bile duct lesions in a 50-year-old woman. Coronal reformation of contrast-

enhanced CT shows marked bile duct wall thickening (arrows).
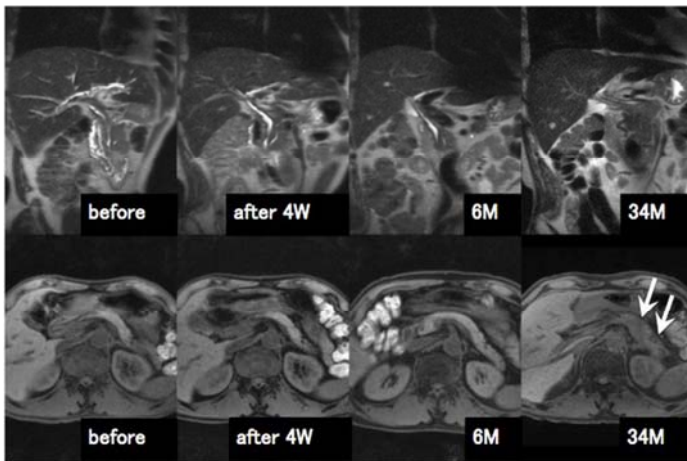
Fig. 5 Bile duct lesions in a 69-year-old man. Oblique coronal T2-weighted images

(**upper column**) before and after corticosteroid therapy images show gradual

improvement of the bile duct lesion. Thirty-four months after corticosteroid

therapy, the bile duct lesion had relapsed. Axial fat saturated T1-weighted images

(**lower column**) show a new pancreatic lesion (white arrows) accompanied by

relapsed bile duct lesion.
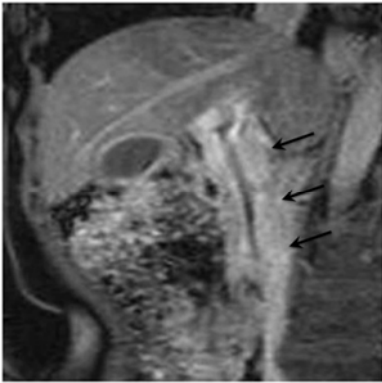
Fig. 6 Bile duct lesions in a 50-year-old woman. Coronal contrast-enhanced MRI shows

prominent wall thickening of the bile duct with significant laminar structure

(arrows).

(a) (b)
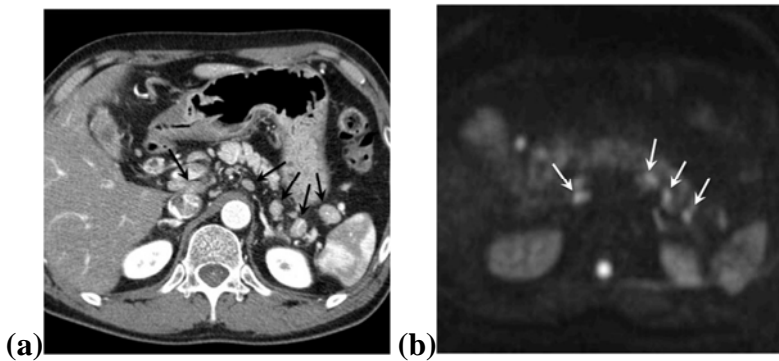
Fig. 7 Peri-pancreatic and para-aortic lymphadenopathy in a 55-year-old man. (a)

Contrast-enhanced CT shows multiple peri-pancreatic lymphadenopathy (arrows).

(b) On diffusion-weighted images, these lesions are detected as high intensity

signals (white arrows).
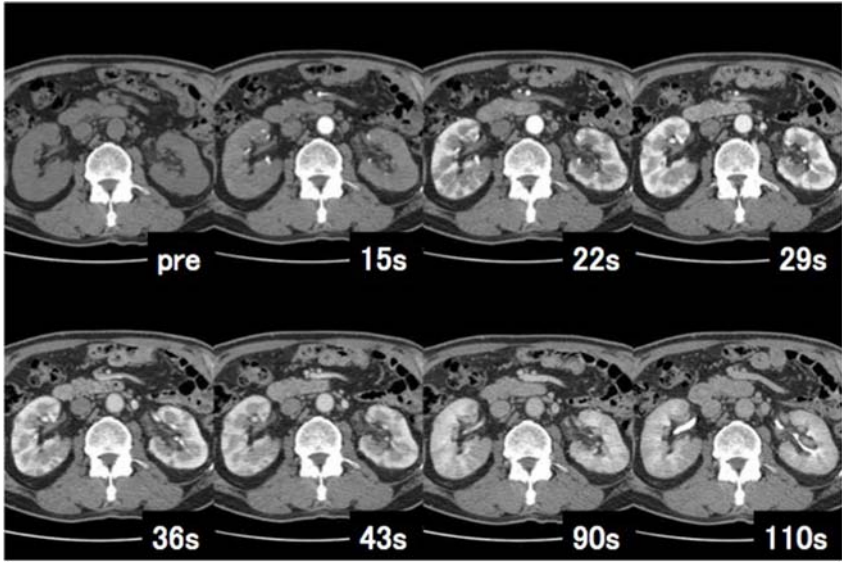
Fig. 8 Renal lesions in a 67-year-old man (same case as in Fig. 1). Multiphase dynamic

contrast-enhanced CT shows multiple poorly enhanced lesions in both kidneys,

and sequential changes in the lesions over time.
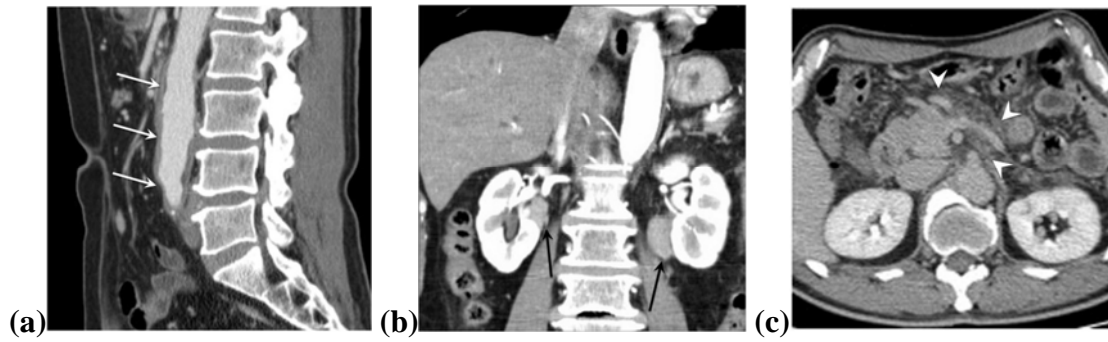
Fig. 9 Retroperitoneal lesions. (a) Sagittal reformation of contrast-enhanced CT shows a

soft tissue mass along the aorta (white arrows). (b) Coronal reformation of

contrast-enhanced CT shows masses around both ureters (arrows). No

hydronephrosis is observed. (c) Axial contrast-enhanced CT shows increased fat

density around superior mesenteric artery and splenic vein (white arrow heads).
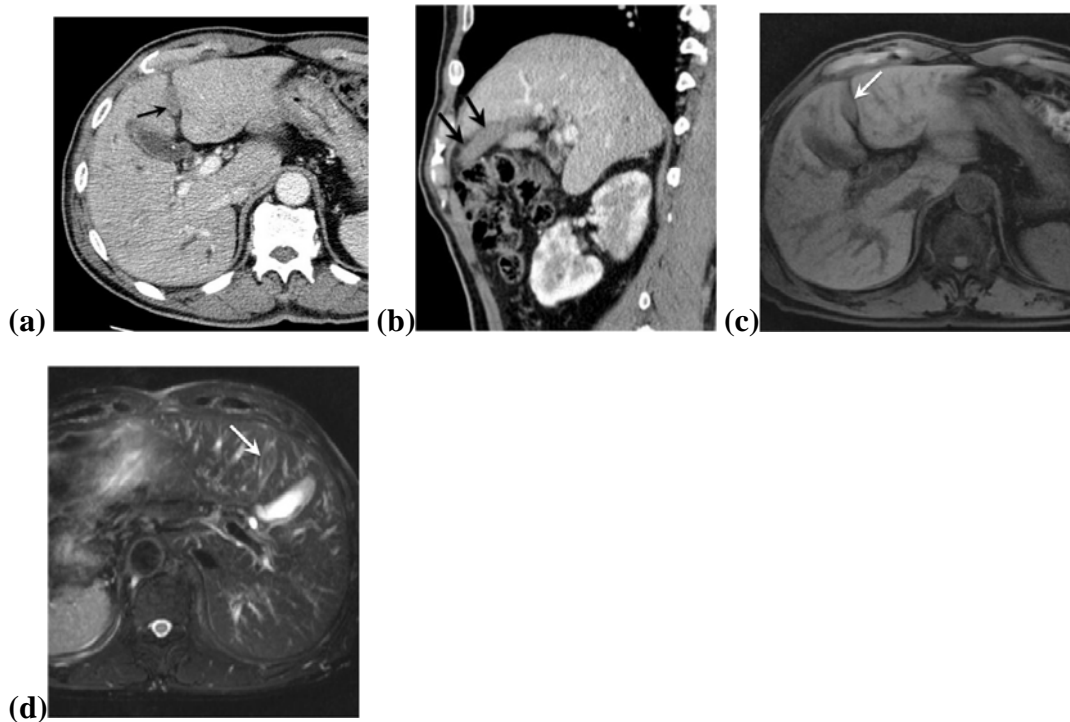
Fig. 10 Lesions in the ligamentum teres. (a) Contrast-enhanced CT shows soft tissues

mass in the ligamentum teres (arrow). (b) Saggital image of contrast-enhanced CT

shows the spindle-shape mass along ligamentum teres (large arrows). (c-d) MR

images show hypointense mass on fat saturated T1-weighted images and

hyperintense mass on fat saturated T2-weighted images (white arrows).

(a) **(b)**
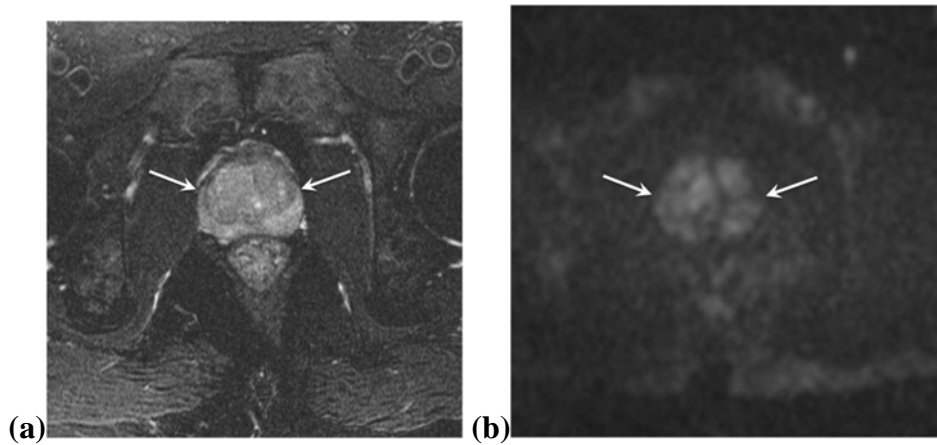
Fig. 11 Prostatic lesions in a 66-year-old man (same case as in **Fig. 9a**). (a) Axial T2-

weighted image with fat saturation shows prostate swelling (white arrows). No

mass lesions can be detected. (b) Diffusion-weighted image shows diffuse high

intensity signal in the prostate (white arrows).